JOURNAL OF AIRCRAFT
Vol. 47, No. 6, November–December 2010

Prediction of Flow Dynamics over Cavities by Detached Eddy Simulation

Niloufar Mahmoudnejad* and Klaus A. Hoffmann†
Wichita State University, Wichita, Kansas 67260-0044

DOI: 10.2514/1.C000255

In this investigation, the flow simulation over different types of cavities (two- and three-dimensional) was performed. The effect of turbulence was implemented with detached-eddy simulation using the Spalart–Allmaras one-equation model. Initially, the flow behavior was investigated and compared for open and closed cavities. In the sound pressure level spectra of the closed cavity, only the broadband noise can be observed, while in the open-cavity case, it consisted of harmonic frequency peaks. Results of the two- and three-dimensional computations were compared with each other and with the available experimental data. It was observed that the results of three-dimensional simulations compared well with the experimental data, and the amplitude of the pressure fluctuations in the two-dimensional case was larger than in the three-dimensional model. Moreover, the pressure fluctuation of the two-dimensional cavity was more periodic than that of the three-dimensional case. Subsequently, a cavity with two circular openings on top, representing a landing gear housing, was investigated. Results show that the existence of these openings changes the characteristics of the flow inside the cavity, and the computed frequencies differ from the results calculated by the Rossiter semi-empirical formula.

Nomenclature

D	=	depth of cavity
e	=	internal energy
f	=	frequency
L	=	length of cavity
M	=	Mach number
P	=	pressure
p'	=	pressure fluctuations
p_{ref}	=	reference pressure (20 μPa)
p_{rms}	=	root mean square sound pressure
Re	=	Reynolds number
St	=	Strouhal number, $St = f_m L/U_\infty$
U	=	velocity
t	=	time
ν	=	kinematic viscosity
$\tilde{\nu}$	=	eddy viscosity
μ	=	absolute (dynamic) viscosity
ρ	=	density
$\tilde{S}$	=	modified vorticity
$\bar{\bar{\tau}}$	=	stress tensor

I. Introduction

PREDICTING flow behavior over cavities has been one of the most interesting areas of research since the 1950s. Many researchers have performed extensive experimental, computational, and analytical investigations. The flowfield of interest includes a large range of Mach numbers and Reynolds numbers with various geometrical considerations, such as length-to-depth ratio L/D and the type of cavity, such as an open cavity or a closed cavity. All of these efforts have been carried out because of the sensitivity of the problem and the presence of undesirable phenomena, such as noise, which is generated by such flows. For example, the International Civil Aviation Organization has determined noise limits and proposed Standards and Recommended Practices regarding aircraft noise (in Annex 16). Therefore, the development of technologies to control noise, such as landing gear noise, is vital. Several examples of such flows include the following: automobile sunroofs and windows, internal weapon bays and wheel wells, pressure vents on the space shuttle cargo bay, and space between railroad wagons. Three classifications of cavities are based on L/D: open-type cavity ($L/D \leq 10$), transitional-type cavity ($10 \leq L/D \leq 13$), and closed-type cavity ($L/D \geq 13$) [1]. Many investigators have carried out experimental and numerical investigations on these three types of cavities. Some of the pioneers who have investigated this phenomenon are Rossiter [2], Sarohia and Massier [3], Krishnamurty [4], Heller and Holmes [5], Gharib and Roshko [6], and Rockwell and Knisely [7]. In 1966, Rossiter carried out an experimental investigation on flow over cavities at subsonic and transonic regimes; this study has been one of the best sources for further investigations, and his proposed formula is commonly used. He found that the unsteady pressures contain both random and periodic components. He suggested that the periodic component is due to an acoustic resonance within the cavity and may be suppressed by positioning a small spoiler at the front of the cavity.

Several researchers focused on the type of turbulence model used in numerical investigations. Shieh and Morris [8] investigated the near-field, unsteady hydrodynamics and acoustics of two- and three-dimensional cavity flows using computational aeroacoustics and unsteady Reynolds-averaged Navier–Stokes (URANS) simulations. They also compared numerical data with experimental data for $L/D = 4.4$ and $M_\infty = 0.6$. Lada and Knotis [9] performed an experimental and computational study to investigate open and closed cavities with and without fluidic control at subsonic and supersonic regimes with $L/D = 2$, 10, 18. Chang and Park [10] conducted a numerical approach to an incompressible cavity flow using a modified detached-eddy simulation (DES) with a k-ε two-equation turbulence model. They compared the numerical data for $L/D = 0.5$, $V_\infty = 40$ m/s with experimental data. Nayyar et al. [11] used large-eddy simulation (LES) and DES to simulate flow ($M_\infty = 0.85$) over a cavity with $L/D = 5$. They compared the numerical data with experimental data and found that both DES and LES performed better than URANS in resolving the higher frequencies and velocity distributions within the cavity. Peng [12] investigated an open-cavity where the flow was computed using both DES and URANS approaches based on a Spalart–Allmaras (SA) model. In comparison with the experimental data, Peng found that the DES produces more accurate results than the URANS computation. Kim et al. [13]

Presented as Paper 2009-3503 at the 27th AIAA Applied Aerodynamics Conference, San Antonio, TX, 22–25 June 2009; received 12 January 2010; revision received 27 April 2010; accepted for publication 9 August 2010.

*Graduate Research Assistant, Department of Aerospace Engineering. Student Member AIAA.

†Marvin J. Gordon Distinguished Professor, Department of Aerospace Engineering. Associate Fellow AIAA.

simulated unsteady, supersonic flow over an open-cavity. They used a k-ε turbulence model and Roe scheme, and compared the data with experimental results for both two- and three-dimensional cases. It was shown that three-dimensional cases were in better agreement to the experimental data than two-dimensional cases. Murray and Ukeiley [14] also investigated subsonic flow over an open cavity with $L/D = 6$, and a Mach number range of 0.19–0.73. A modified quadratic stochastic estimation with proper orthogonal decomposition (POD) was applied to the data to demonstrate how the temporal dynamics of the wall pressure fluctuations are related to the downstream propagation and impingement of vortices traveling through the cavity shear layer. Boydston and Squires [15] computed the flow over a rectangular cavity using the SA turbulence model and DES. The L/D used was 4.5. Langtry and Spalart [16] examined whether unsteady flow computations using either URANS or DES could predict the cavity oscillations that were measured in a wind tunnel test and the subsequent reduction due to the introductions of the baffles within the cavity. They found that both URANS and DES were similar in predicting the dominant oscillation.

Some investigators have attempted to develop higher-order numerical schemes to predict the flow characteristics over cavities. Shieh and Morris [17] developed a parallel, multiblock, high-order accurate code for cavity-noise prediction. They examined the effects of changing the incoming boundary layer thickness on pressure fluctuations. Rona and Brooksbank [18] used an explicit time-marching, second-order finite-volume scheme to generate time-dependent benchmark cavity-flow data. The focused flow regime was supersonic.

Zhang et al. [19] studied compressible flows over cavities with a wide range of L/D, both experimentally and computationally. The effect of the upstream separation wake on the downstream recompression wakes was investigated. It was shown that the installation of tubes along the two side walls of the cavity is the most effective way to reduce the adverse pressure gradient along the cavity centerline. Zhang and Naguib [20] also investigated unsteady oscillation in a low-Mach, shallow-cavity flow with different Reynolds numbers and aspect ratios (3.4–9.7). Chung [1] performed experiments to study the effect of cavity geometry and Mach number on the characteristics of compressible cavity flows. The study indicated that in open-type cavity the amplitude of surface pressure fluctuations increased toward the rear face, while in closed-type cavity a minor peak near the middle of the cavity floor was observed. It was also shown that more intense surface pressure fluctuations were induced at the cavity floor in transitional-type cavity. Experimental efforts of Little et al. [21] provided preliminary results of flow structure and acoustic signature in controlled and baseline subsonic cavity flows.

Several investigators have concentrated on noise reduction and control. Sarohia and Massier [3] conducted experiments on axisymmetric shallow-cavity flows. Their goal was to provide methods to reduce cavity noise. Results showed that continuous injection of a fluid mass at the base of the cavity has a stabilizing effect on cavity shear flows, and it can be an effective means of suppressing cavity-flow noise. Vakili and Gauthier [22] used a mass injection upstream of a cavity to control shear flow across the cavity for reducing or eliminating cavity-flow oscillations. Heo and Lee [23] numerically investigated the effects of cover plates existing on the edges of a rectangular open cavity. It was shown that the cover plates on the edges of the cavity change the frequency, sound pressure level, and directivity of noise and induce the transition of the resonance mode. Guo and Yamamato [24] carried out an experimental investigation on full-scale Boeing-737 landing gear noise.

With this background, the current effort is directed toward simulation of flow over different types of cavities in subsonic and transonic regimes.

II. Simulation Methodology

A. Governing Equations and CFD Solver

The governing equations are the unsteady, compressible Navier–Stokes equations, composed of the conservations of mass, momentum, and energy.

1) Continuity equation:

$$\frac{\partial \rho}{\partial t} + \nabla \cdot \rho \mathbf{U} = 0 \tag{1}$$

2) Momentum equation:

$$\frac{\partial \rho \mathbf{U}}{\partial t} + \nabla \cdot \rho \mathbf{U} \otimes \mathbf{U} + p\bar{\bar{I}} = \nabla \cdot \bar{\bar{\tau}} \tag{2}$$

3) Energy equation:

$$\frac{\partial \rho e_t}{\partial t} + \nabla \cdot [\rho e_t + p\mathbf{U}] = \nabla \cdot \mathbf{U} \cdot \bar{\bar{\tau}} - \nabla \cdot \mathbf{Q} \tag{3}$$

Numerical simulations were conducted using the CFD code Cobalt, which is an unstructured finite-volume code, using a cell-centered formulation. It is based on Godunov's first-order accurate, finite-volume, exact Riemann solution method. The exact Riemann solver is replaced with an inviscid flux function that alleviates the inherent shortcomings of Riemann methods, namely the *slowly moving shock* and *carbuncle* problems, while retaining their inherent advantages, most notably the exact capture of stationary contact surfaces. Second-order spatial accuracy is achieved via upwind-biased reconstruction based on least-squares gradients.[‡] This compressible flow solver has been validated on several problems by Strang et al. [25], Forsythe et al. [26], Viswanathan et al. [27], and Boydston and Squires [15]. Cobalt provides both Reynolds-averaged Navier–Stokes (RANS) and DES approaches for turbulent flows. Several turbulence models are available in Cobalt, including Spalart–Allmaras one-equation turbulence model, DES based on SA, Menter's baseline, Menter's shear stress transport (SST), DES based on SST, Wilcox's 1998 k-ω model, SA rotation correction (SARC), and DES with SARC [28]. Total variation diminishing limiters are used to limit extremes at cell faces. ParMETIS is used to implement parallel processing and domain decomposition and the message passing interface manages communication between processors.

B. Turbulence Model

Detached-eddy simulation is a hybrid technique proposed by Spalart et al. [29] in 1997 as a numerically feasible and reasonably accurate approach for predicting massively separated flows [30]. This model is a combination of RANS and LES, whereby the model switches to a subgrid scale formulation in regions sufficiently fine for LES calculations. In this technique, LES mode is activated in regions where it is expected to have less accurate results of RANS mode or the turbulent length scale goes over the grid dimension. The model activates the RANS mode for near wall regions. DES model combines the advantages of these two models which are less simulation costs in RANS and ability of LES to capture unsteady flow structures. However, in hybrid RANS/LES schemes the transmission of the information between LES and RANS zones is not easy [31]. In the RANS regions only data related to the mean flow is available, and the Reynolds shear stresses are supported by the turbulence model. In the LES regions the turbulent eddies are present to support the turbulent momentum transport. The generation of these eddies is a critical feature in determining the success and accuracy of the hybrid method and their absence may degrade the reliability of the method [31]. Also in boundary layer region, as the grid spacing in direction of parallel to the wall becomes smaller than half of the boundary layer thickness, the eddy viscosity becomes smaller than its RANS level, though without allowing LES behavior. Subsequently, the solution creates insufficient Reynolds stresses which leads to early separation or under prediction of skin friction [30]. Obviously, each turbulence model has its own drawbacks and benefits. In practice, DES has been successful in separated flows. In the current investigation, DES was performed using the SA one-equation model. DES97 is a DES based on the SA one-equation RANS model. The transport equation in this model is:

[‡]Additional data available online at http://www.cobaltcfd.com/index.php/site/software/cobalt [accessed May 2009].

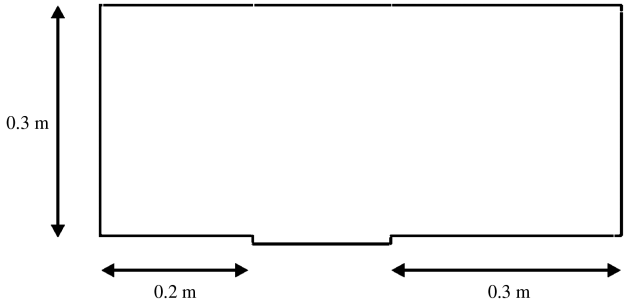

Fig. 1 Two-dimensional closed-cavity configuration ($L/D = 18$).

$$\frac{D\tilde{\nu}}{Dt} = c_{b1}\tilde{S}\,\tilde{\nu} - c_{\omega 1} f_{\omega}\left[\frac{\tilde{\nu}}{d}\right]^2 + \frac{1}{\sigma}[\nabla\cdot\nu + \tilde{\nu}\nabla\tilde{\nu} + c_{b2}\nabla\tilde{\nu}^2] \qquad (4)$$

where $c_{b1}\tilde{S}\,\tilde{\nu}$ is the production term, $\frac{1}{\sigma}[\nabla\cdot\nu + \tilde{\nu}\nabla\tilde{\nu} + c_{b2}\nabla\tilde{\nu}^2]$ is the diffusion term, $c_{\omega 1} f_{\omega}[\frac{\tilde{\nu}}{d}]^2$ is the destruction term, $\tilde{\nu}$ is the eddy viscosity, d is the distant to the wall, and $\tilde{S}$ is the modified vorticity. More details about this turbulence model can be found in [29].

III. Simulation Models

In the present research, three two-dimensional and two three-dimensional configurations were modeled and investigated to better understand flow behavior over the cavities.

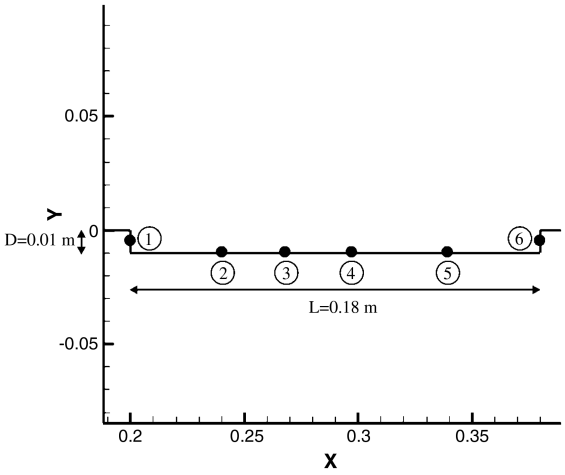

Fig. 2 Sensor locations at closed cavity ($L/D = 18$).

A. Two-Dimensional Models

Two-dimensional simulations provide some insight about behavior of the flow over cavities, with the advantage in computation time and memory consumption. Previous investigations performed by Kim et al. [13] show that the amplitude of the pressure fluctuation in the results from the two-dimensional simulation is more than twice that from the three-dimensional simulation. There is also an overall increase in the sound pressure level (SPL), however, the form of the SPL along the walls is very similar in both cases. These differences are due to the three-dimensional effects and the structure of the flow in the shear layer and within the cavity. In general, the two-dimensional results can be used to estimate the longitudinal mode of the cavity flow. Closed-cavity flows usually occur in shallow cavities where $L/D \geq 13$ [32]. In the present investigation, a two-dimensional cavity with $L/D = 18$ was used. A schematic presentation of the cavity is shown in Figs. 1 and 2. The cavity contains about 380,000 cells in which grid clustering near wall surfaces was implemented. The two-dimensional grid system is illustrated in Fig. 3. The time increment,Δt, used in this simulation was 2×10^{-7} sec.

Open-cavity flows generally occur in deep cavities with $L/D < 10$ [32]. In the current study, an open cavity with $L/D = 4$ and another with $L/D = 5$were investigated. The two-dimensional configuration and grid systems of the first model ($L/D = 4$) are shown in Figs. 4–6. As shown in these figures, grid clustering near the wall surfaces has been implemented. The total number of grid points for this case was about 158,000. The time increment, Δt, used in this simulation was 2×10^{-7} sec. The second model ($L/D = 5$) configuration was exactly the same as the first, except for the length of the cavity. This configuration was studied to compare the two- and three-dimensionality effects. The overall grid system is shown in Fig. 7. The total number of grid cells was about 560,000, and the time increment, Δt, was the same as the previous open cavity.

B. Three-Dimensional Models

The first three-dimensional model was a benchmark problem that compared numerical data with available experimental data. The flowfield over a backstep computed by Cobalt was validated previously by Dietiker and Hoffmann [33], and in the current effort, the flowfield over the cavity has been validated. The geometry contains a rectangular cavity with $L/D = 5$, which corresponds to an open-cavity flowfield. The overall computational domain is 1.2954 by 0.3048 by 1.143 m. The cavity has dimensions of 0.508 by 0.1016 by 0.1016 m. The overall geometry is shown in Fig. 8, and the three-dimensional grid system is illustrated in Fig. 9. The grid is composed of about two million cells. The cavity contains 450,000 (150× 60 × 50) grid nodes. The time increment Δt used in this simulation was 3×10^{-7} sec.

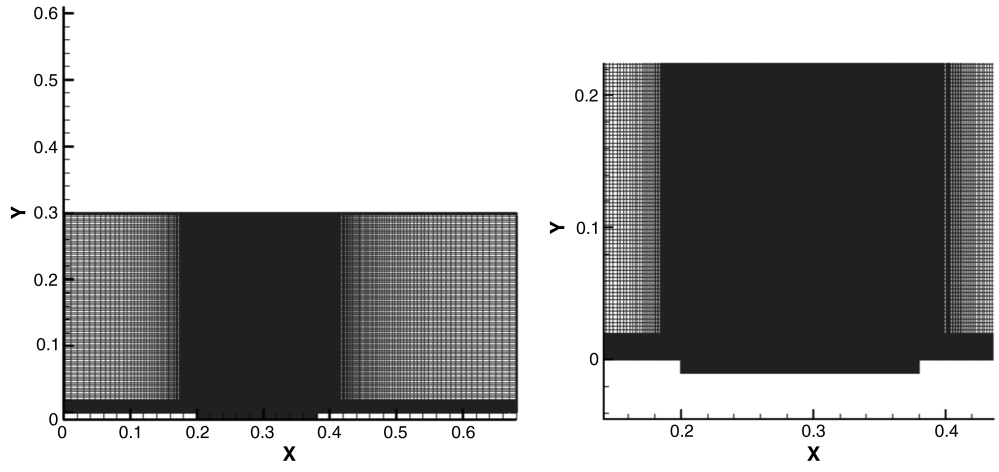

a) b)

Fig. 3 Illustration of computational mesh for closed cavity ($L/D = 18$); a) overall view of structural mesh, and b) clustered mesh over cavity.

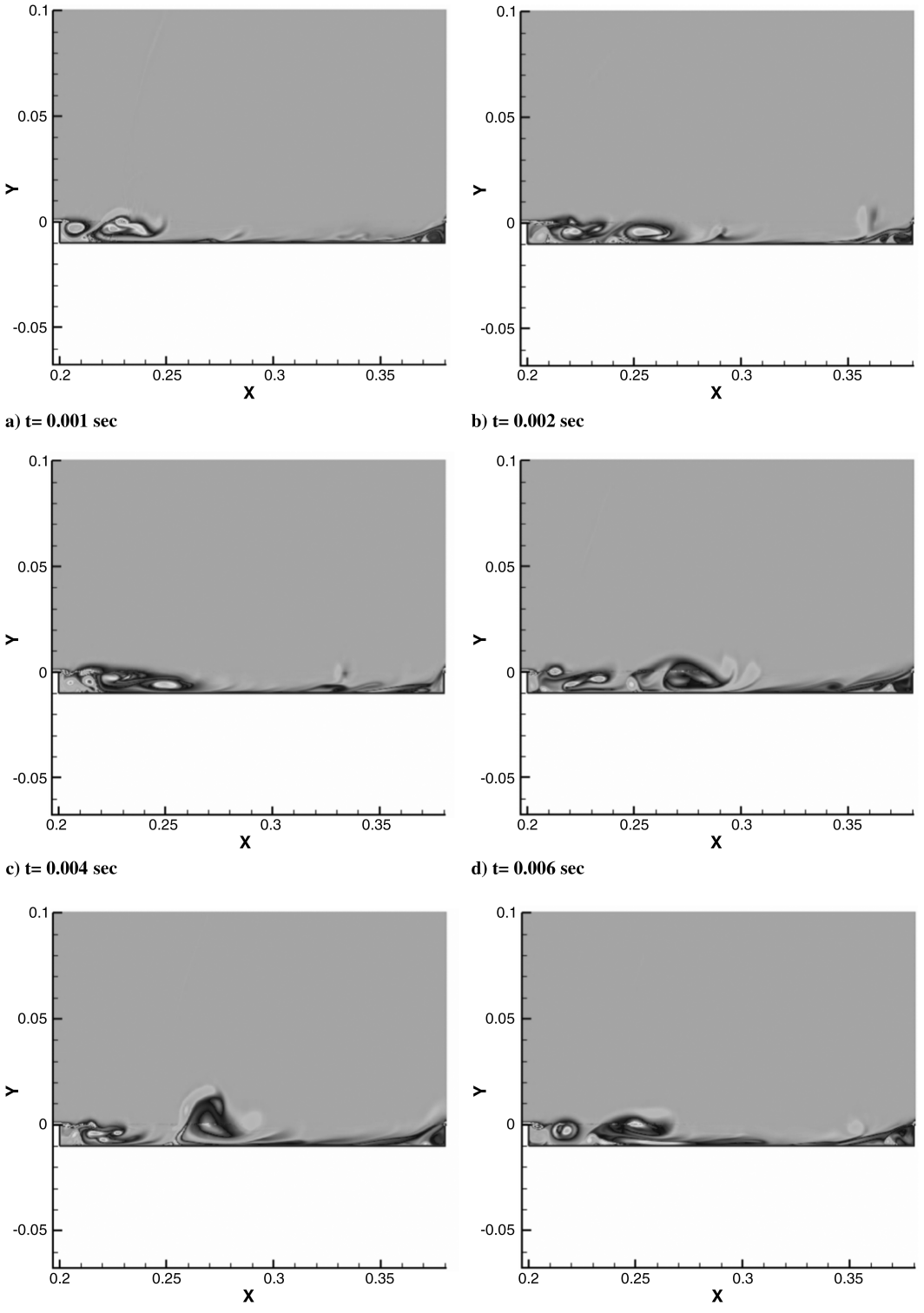

Fig. 4 Two-dimensional open-cavity configuration ($L/D = 18$).

The second three-dimensional problem setup consisted of a rectangular parallelepiped ($L/D = 2$ and $L/W = 1$) with two circular openings on top ($r = 0.1$ m). This represents a model for landing gear housing. The region above the cavity was modeled as a rectangular unstructured grid. The total number of elements is about three million. The freestream Mach number was assumed to be 0.7. An atmospheric condition was imposed to the freestream flow. Figure 10 illustrates the model geometry and the grid system. The interior of the cavity was meshed with tetrahedral cells. Grid-point clustering was implemented near the walls. The time increment, Δt, used in this simulation was 2×10^{-6} sec.

In all models, the grid system was generated by Gridgen.[§] For two- and three-dimensional grids, it can generate structured hex, unstructured tet, and hybrid meshes. Its data can be exported to about

[§]Additional data available online at http://www.pointwise.com/gridgen [accessed May 2009].

33 flow solvers. The geometry can also be imported from about 15 file formats such as CATIA, IGES, PATRAN, NASTRAN, etc.

IV. Results and Discussions

The pressure fluctuations were recorded at different locations and each time step for all cases. Results focused on the pressure perturbation, p', which propagates as waves and can be detected by humans. For harmonic pressure fluctuations, the audio range is about 20 Hz $\leq f \leq$ 20 kHz [34].

For accurate prediction of the unsteady flowfield and behavior of the flow characteristics, the sound pressure level at different locations was assessed. The sound pressure level can indicate the overall increase in the amplitude of the pressure fluctuations and is defined as follows:

$$\text{SPL} = 10\log_{10}\left(\frac{p_{\text{rms}}^2}{p_{\text{ref}}^2}\right) = 20\log_{10}\left(\frac{P_{\text{rms}}}{P_{\text{ref}}}\right) \tag{5}$$

which is measured in decibels (dBs). The lowest sound pressure possible to hear (p_{ref} or threshold of human hearing) is approximately 20 μPa, which is valid for sound that propagates in gases. In other media, p_{ref} will be 1 μPa.

In the current research, SPL was calculated by fast Fourier transform function using the recorded pressures over time at each location. This is a faster version of the discrete Fourier transform

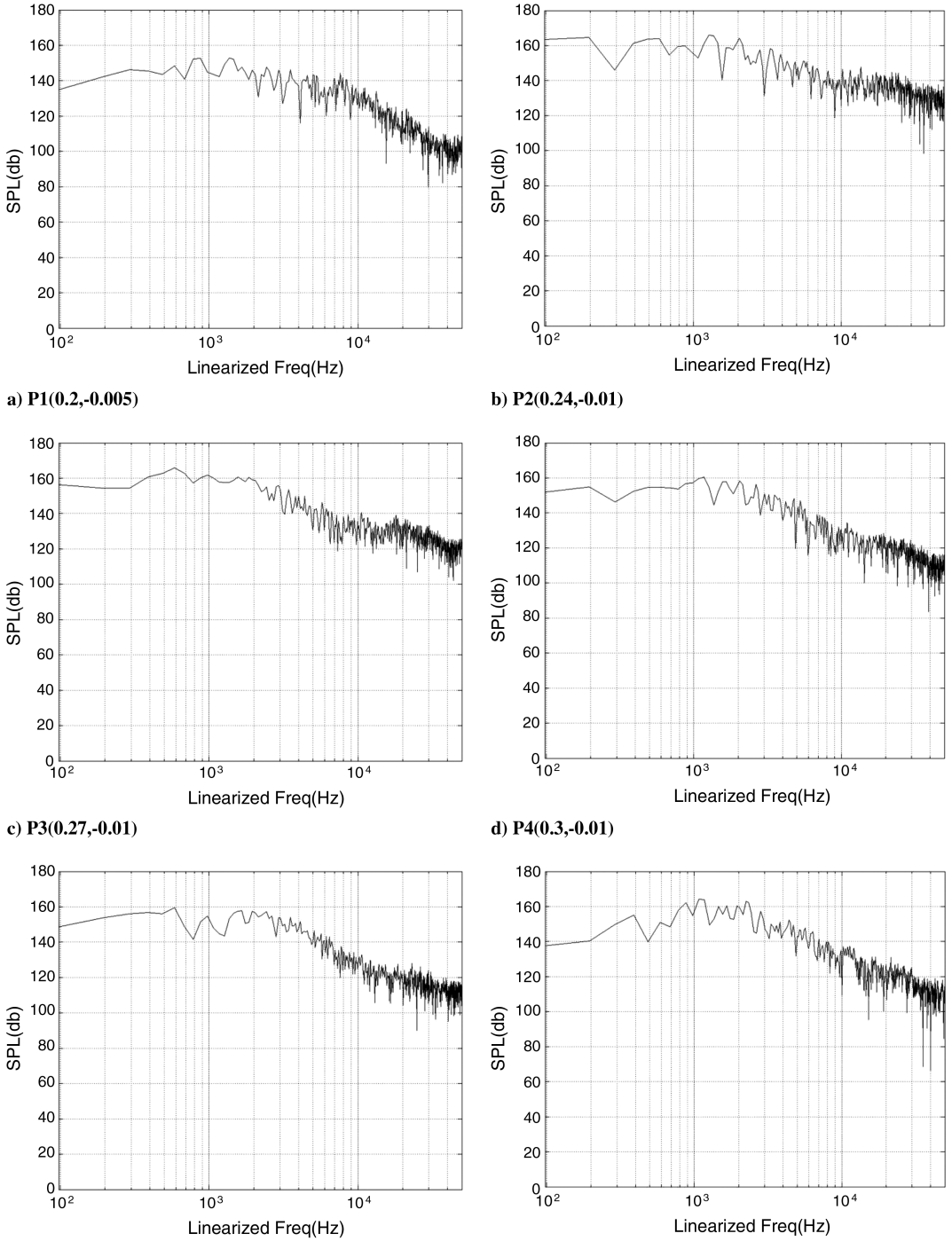

Fig. 5 Sensor locations at open cavity ($L/D = 4$).

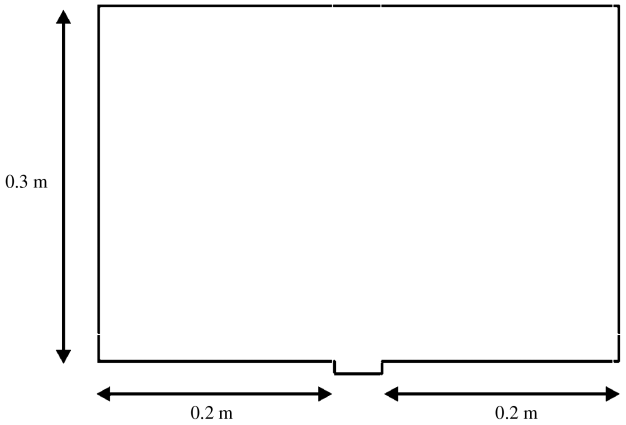

Fig. 6 Illustration of computational mesh for open cavity ($L/D = 4$); a) overall view of structured mesh, b) clustered mesh over cavity.

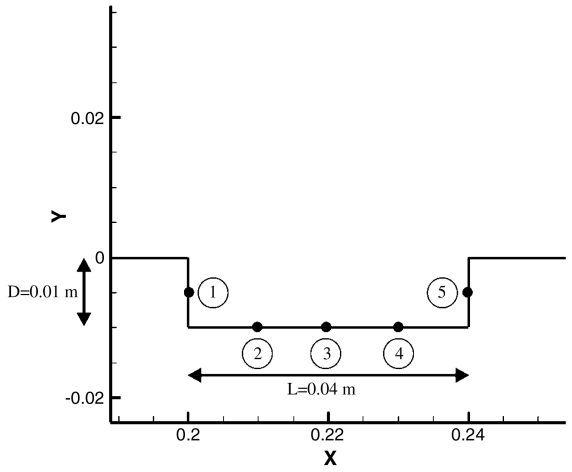

Fig. 7 Two-dimensional open-cavity grid system ($L/D = 5$).

function that uses the same algorithms but much less time in execution. Matlab has an effective tool for computing the Fourier transform of a signal, which was used in this study.

The acoustic field for cavities can be estimated by a semi-empirical formulation, which was developed by Rossiter [2]:

$$St = \frac{f_m L}{U_\infty} = \frac{m - \alpha}{M_\infty + \frac{1}{k}} \tag{6}$$

The Rossiter equation was modified by Heller and Bliss [35]:

$$St = \frac{f_m L}{U_\infty} = \frac{m - \alpha}{M_\infty / \sqrt{1 + \frac{\gamma - 1}{2} M_\infty^2} + \frac{1}{k}} \tag{7}$$

Heller and Bliss found that the speed of sound in the cavity is equal to the stagnation speed of sound in the freestream flow. In Eq. (7), f_m is the frequency of oscillation, U_∞ is the freestream speed, L is the cavity length, m is the Rossiter mode number, α and k are empirical values, and M_∞ is the freestream Mach number. Rossiter found that k is a constant equal to 0.57, and α is a function of L/D and is related to the phase between the vortices within the shear layer and the upstream traveling pressure waves within the cavity [32]. St is the Strouhal number, which is a nondimensionalized measure of the cavity resonant frequency.

The unsteady cavity flowfield consists of both random and periodic components of pressure fluctuations. Tracy and Plentovich [36] performed an investigation showing that the SPL spectra for open- and closed-cavity flows typically are as illustrated in Fig. 11. To study these phenomena, two-dimensional cavities were investigated: one with $L/D = 4$, which corresponds to an open-cavity type flow, and the other one with $L/D = 18$, which falls in the closed-cavity type flow.

Another important issue in cavity study that should be noted is the types of oscillation of the flow within the cavity. There are two different types of oscillations [37]: wake mode and shear layer mode. Several investigators have carried out experimental and numerical investigations which clarified the characteristics of the wake and shear layer modes. Gharib and Roshko [6] were the first that noticed the wake mode phenomenon and the first description of feedback process was proposed by Rossiter [2]. Later, Rowley et al. [38] described the interaction of the mixing layer and the pressure field as shear layer mode which was characterized by the feedback process proposed by Rossiter. In shear layer mode, the vorticity is rolled up and the acoustic waves, at the downstream cavity edge, are impinged and scattered. Upstream acoustic wave propagates and the shear layer approaches to the acoustic disturbances [37]. Along the shear layer, the vortical disturbances propagate and grow. However, the flow within the cavity is quiescent. A relatively weak and steady vortex is generated in the downstream half of the cavity which was found by Roshko [39] for the first time. This vortex induces vorticity along the walls. Apparently, the interaction of the flow inside the cavity with the shear layer is weak.

By increasing the length or depth of the cavity and/or Mach and Reynolds numbers, the cavity oscillations behavior is changed [37]. Gharib and Roshko [6] observed that instead of a free shear layer behind a bluff body, the oscillating flow is similar to a wake. Colonius et al. [40] showed that the transition from shear layer to wake mode

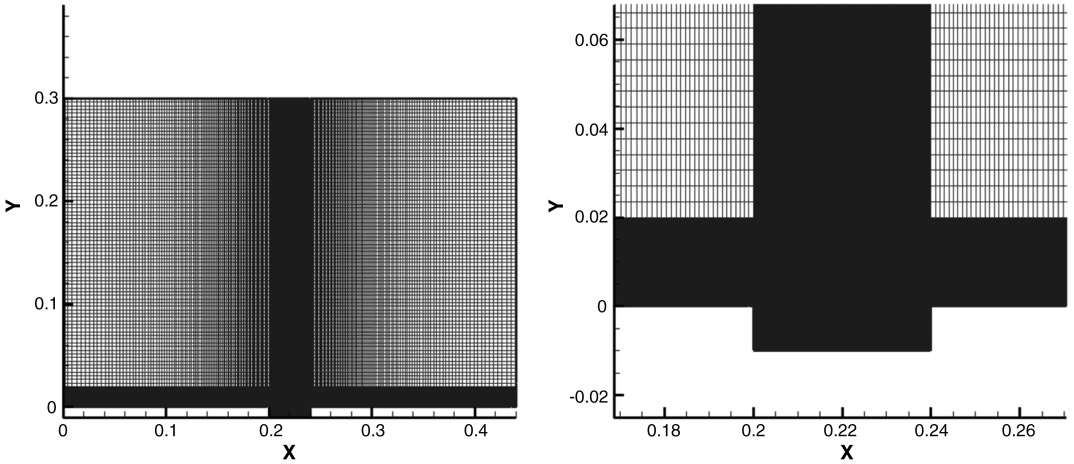

a) b)

Fig. 8 Three-dimensional rectangular cavity ($L/D = 5$); a) general configuration, b) sensor locations.

occurs when the length of the cavity is increased relative to the upstream boundary layer thickness and as Mach number increased with other parameters remaining constant. At the leading edge of the cavity, a vortex begins to form. It grows until its size is almost the size of the entire cavity. At the same time, the irrotational freestream fluid directs into the cavity and collides on the walls. Therefore, vorticity is generated between the upstream cavity wall and the vortex. Subsequently, the vortex is shed from the leading edge and ejected from the cavity. This vortex causes the flow separate from the upstream of the cavity. The periodic ejection of the vortex from the cavity leads to an increased drag. Colonius et al. [40] found that the upstream separation is a key feature of the transition to wake mode. They showed that the spectra of the resonant instabilities in wake mode are very different from those of the shear layer mode. For cavity oscillations in shear layer mode, the flow is nearly parallel, while in wake mode the flow is far from parallel and the disturbances are not small. The radiated acoustic field is also different in two modes. In shear layer mode, the acoustic field, centered at the downstream cavity edge, is dominated by a single frequency, while in wake mode the acoustic field displays a wide range of frequencies.

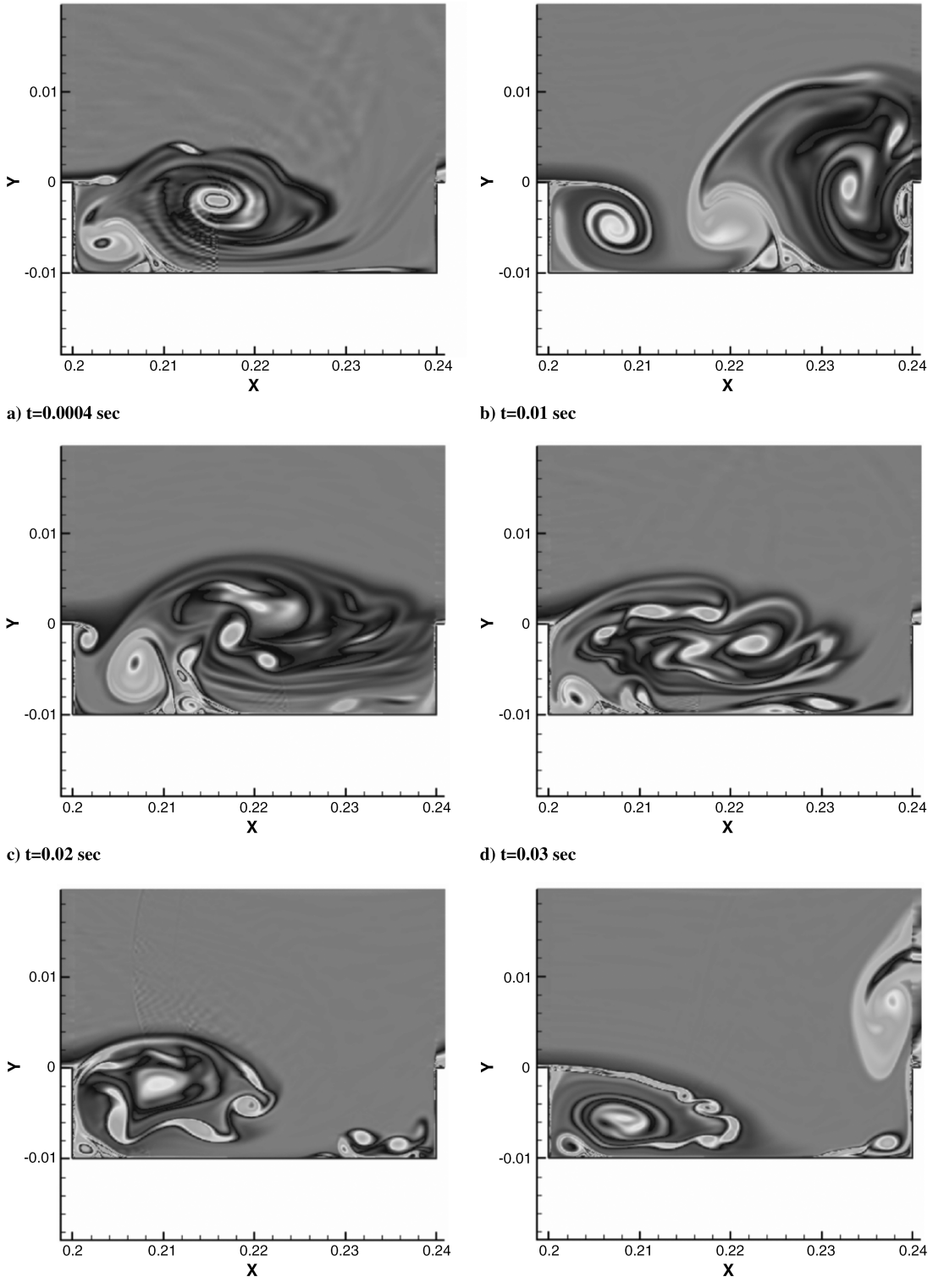

a) t=0.0004 sec b) t=0.01 sec

c) t=0.02 sec d) t=0.03 sec

e) t=0.04 sec f) t=0.05 sec

Fig. 9 Three-dimensional grid system of rectangular cavity ($L/D = 5$); a) general overview, b) clustered mesh over cavity.

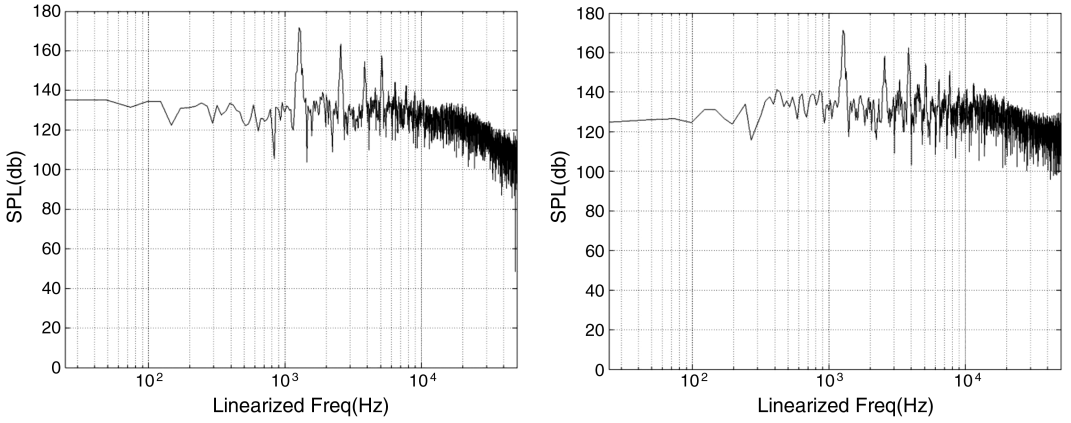

a) P1(0.2,-0.005)

b) P2(0.21,-0.01)

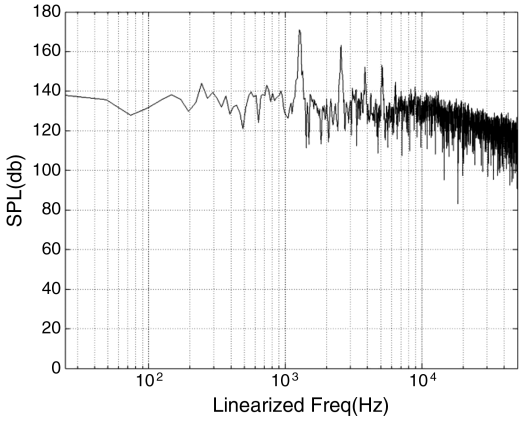

c) P3(0.22,-0.01)

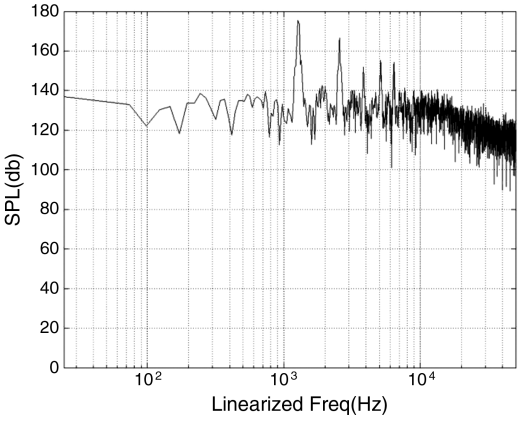

d) P4(0.23,-0.01)

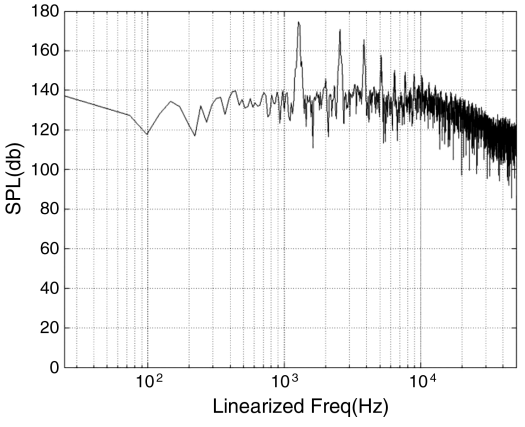

e) P5(0.24,-0.05)

Fig. 10 Three-dimensional cavity with two holes; a) general configuration, b) grid system.

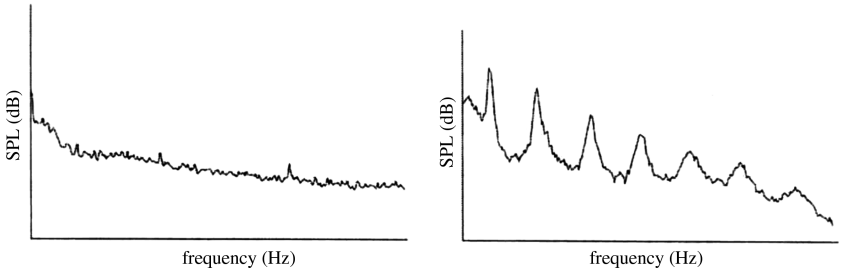

a) Closed flow b) Open flow

Fig. 11 Typical SPL spectra for closed and open-cavity flows [36].

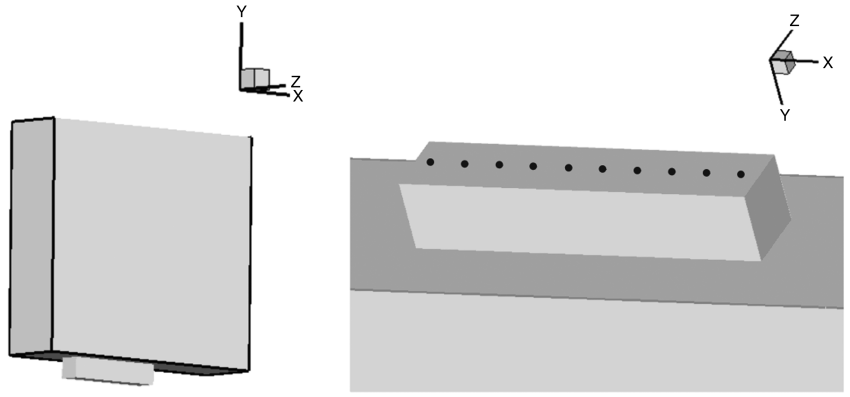

a) b)

Fig. 12 Snapshots of instantaneous vorticity contours for closed cavity ($L/D = 18$).

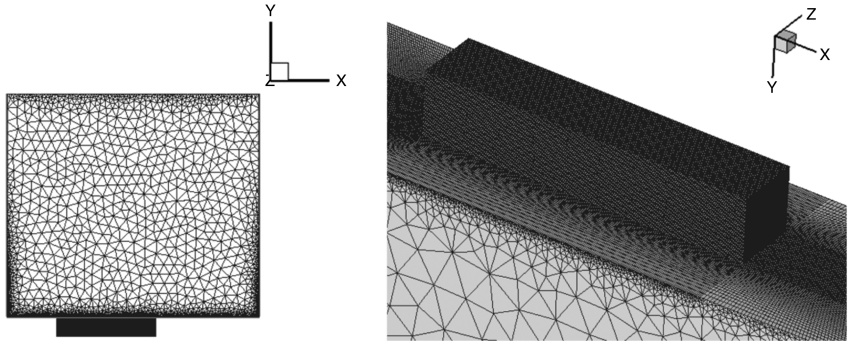

a) b)

Fig. 13 SPL spectra at different locations for closed cavity ($L/D = 18$).

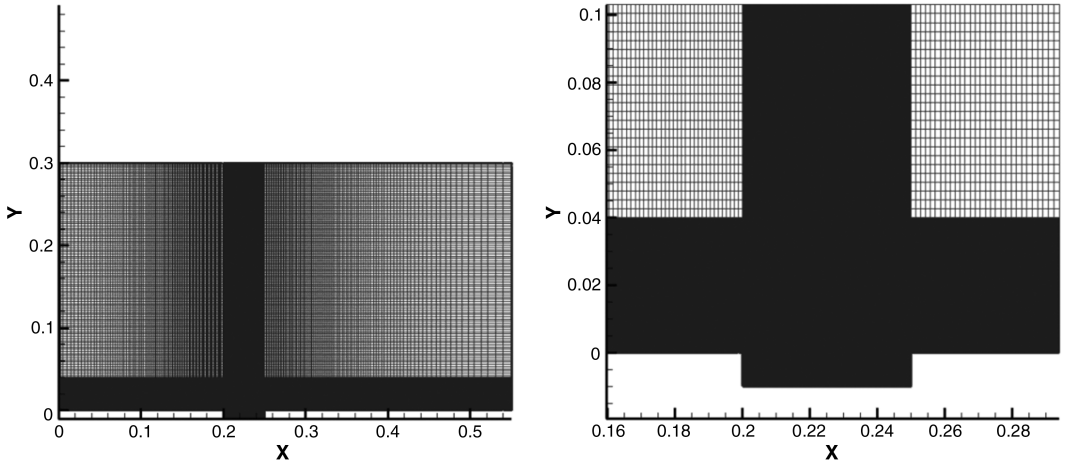

a) b)

Fig. 14 Snapshots of instantaneous vorticity contours for open cavity ($L/D = 4$).

However, the presence of a wake mode is not observed in experimental efforts of compressible cavity flows [34]. Shieh and Morris [8] performed a three-dimensional study and did not observe any wake mode transition for a configuration that they had studied in two dimensions. In three-dimensional case, the turbulent mixing between counter-rotating vortices in the recirculation zone is modified by the vortex stretching and this prevents transition to the wake mode [34].

A. Two-Dimensional Closed Cavity ($L/D = 18$)

For the current geometry, the atmospheric condition with Mach number 0.7 was imposed. The closed-cavity acts similar to a combination of forward and backward steps. Figure 12 illustrates the vorticity contours at different time levels. The shear layer attaches to

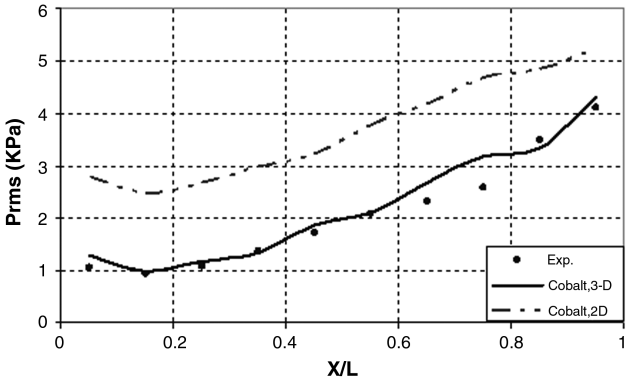

Fig. 15 SPL spectra at sensor locations for open cavity ($L/D = 4$).

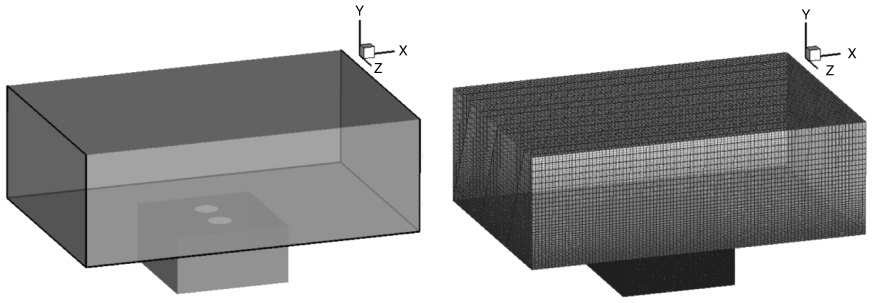

a) b)

Fig. 16 Pressure (rms) fluctuations along cavity floor.

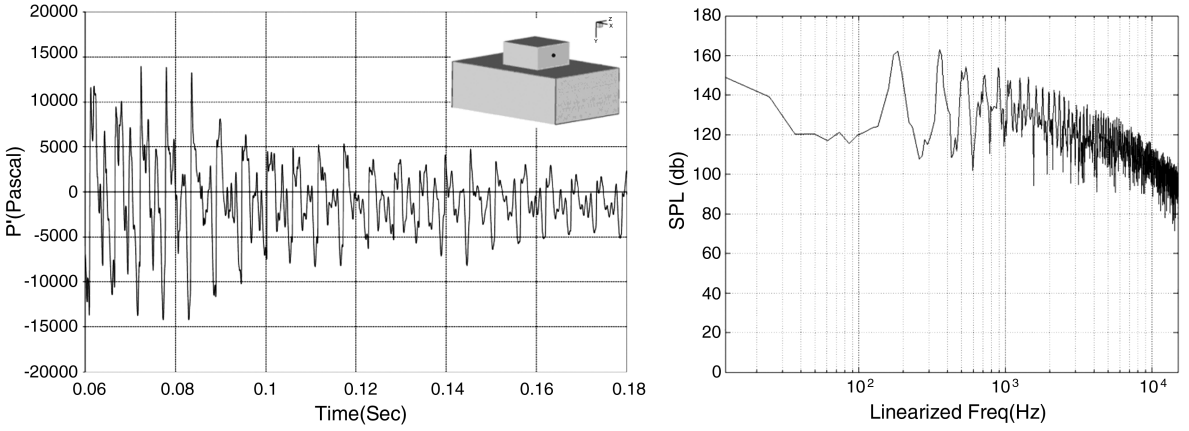

a) P(0.5,-0.25,0)

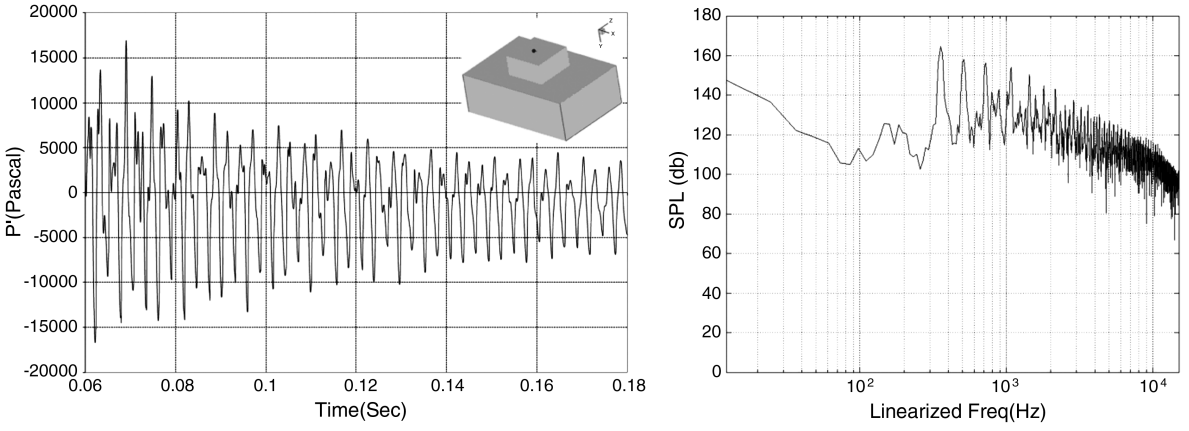

b) P(0,-0.5,0)

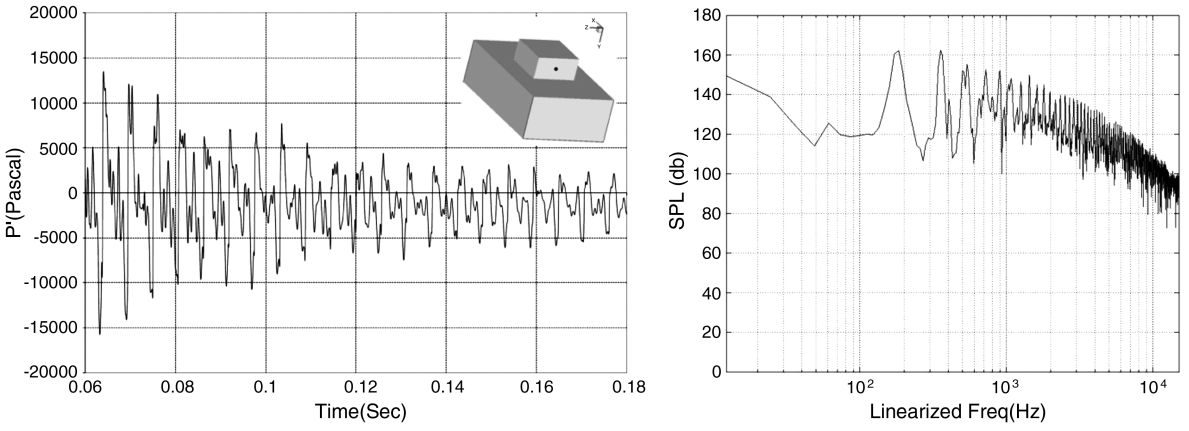

c) P(-0.5,-0.25,0)

Fig. 17 Time history of pressure fluctuations and SPL spectrum at different locations of the three-dimensional cavity with two holes.

the cavity floor and again separates from the floor and extends to the cavity rear wall and trailing edge. Therefore, two recirculating regions are observed.

For this type of the cavity, the pressure distribution consists of different regions. A low expansion region can be observed behind the front face, an increase because of the shear layer impingement, a flat pressure distribution in the impingement region, and a maximum ahead of the rear face [41]. Baysal and Stallings [42] showed that in comparison with the open cavity, the larger pressure can be found on the rear face of the closed cavity and smaller pressure is detected on the front face of the cavity. This leads to a higher drag for closed-cavity flow. The SPL spectra at different locations are shown separately in Fig. 13. In closed-flow cavities, the random component of the pressure is more dominant than the periodic component. In the SPL spectra, only the broadband noise can be seen, and there are generally two or more peaks of similar magnitude in the amplitude.

B. Two-Dimensional Open Cavity ($L/D = 4$)

The freestream Mach number of 0.7 and atmospheric conditions were used for flow simulation over an open cavity with $L/D = 4$. In the three-dimensional open cavity, the shear layer separates from the cavity leading edge and subsequently reattaches to the cavity trailing edge, which forms a single circulation region shifted toward the rear wall of the cavity. However, in the two-dimensional case, more than one vortex, which is very much time dependent, can be observed. It is apparent that generation, destruction, and merging of these vortices will affect the pressure fluctuation and overall SPL.

Vorticity contours at different time levels are shown in Fig. 14. Two-dimensional behavior causes the transition to a wake mode. However, as stated previously, such a wake mode transition does not exist in the three-dimensional model. As shown, the flow separates from the leading edge of the cavity and vortical flow begins to develop. First snapshot shows two resident vortices within the cavity. The one near the front wall of the cavity stays almost stationary as time goes by, while the other vortex grows rapidly to occupy the entire cavity. The rolled up flow travels toward the trailing edge of the cavity, part of which continues to travel downstream and the other which generates the recirculating region. This cycle is repeated over time.

SPL spectra at different locations are shown separately in Fig. 15. The SPL spectra in this type of cavity consist of harmonic frequency peaks, which are clearly observed. As Krishnamurty [4], and Rossiter [2] have shown, the flow in this case is dominated by periodic pressure fluctuations, while the random component is less significant.

C. Two- and Three-Dimensional Rectangular Cavity ($L/D = 5$)

The experimental results, which were carried out by Henshaw at QinetiQ [43], were used to assess the accuracy of the numerical results. A Mach number of 0.85 with static pressure of 63,200 Pa and temperature of 300 K were imposed on the model. The freestream Mach number corresponds to a freestream velocity of $U_\infty = 295.111$ (m/s), and the Reynolds number based on the cavity length is about 7.5 million.

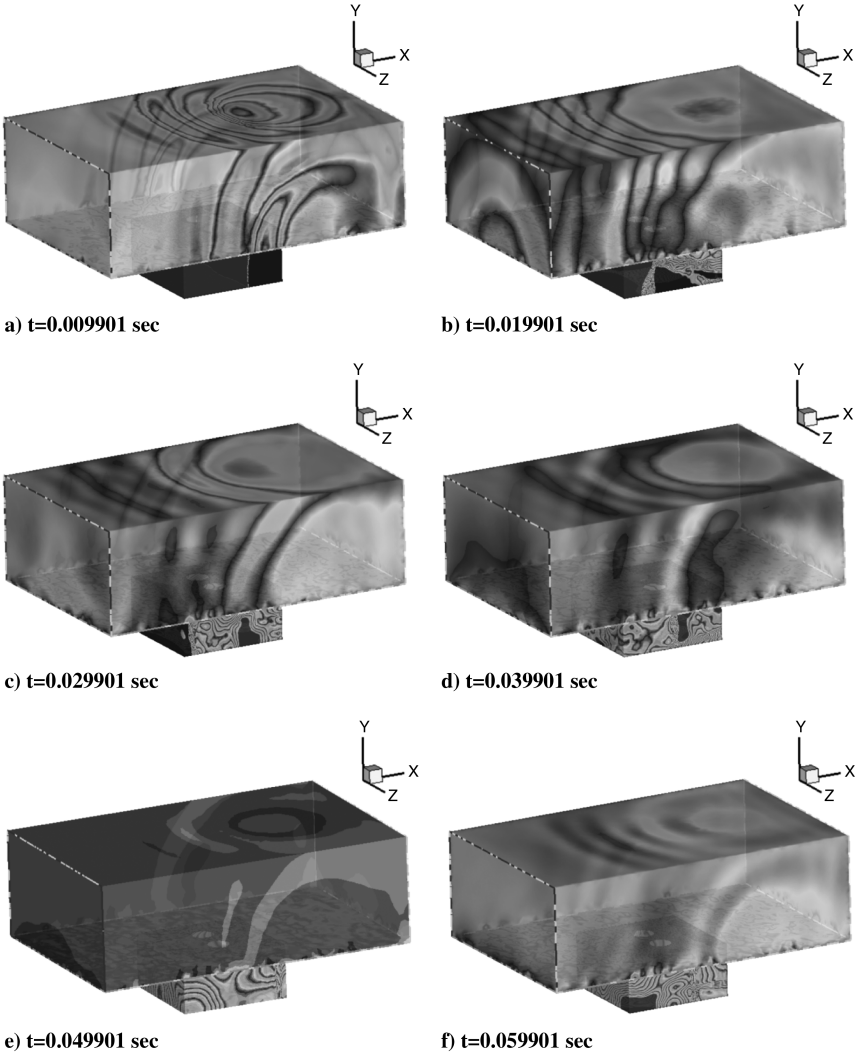

Fig. 18 Snapshots of Schlieren-like pressure contour of the three-dimensional cavity with two holes.

For validation, ten sensor points were located along the cavity floor, as shown in Fig. 12b. The numerical data was measured every 1.5×10^{-5} sec. To obtain the mean flow properties and to prevent any effects of the initial flow conditions, the first 10,000 time steps have been removed from the results. To understand the three-dimensional effects, a two-dimensional model with the same operating conditions was also investigated. Figure 16 shows rms pressure along the cavity floor for experimental two- and three-dimensional models. It was anticipated that the results of the two-dimensional model would be higher than the three-dimensional model but with similar trends. The results of three-dimensional computation are in good agreement with experimental data. It should be noted that the pressure fluctuation of the two-dimensional cavity is more periodic than that of the three-dimensional case, and the amplitude of the fluctuations is larger as shown in [8] as well. The periodic component is due to the acoustic resonance within the cavity. After a small decrease in rms pressure, an increasing tendency along the cavity floor is observed. The sudden drop in pressure near the front wall of the cavity is due to the flow separation at the initial impingement of the vortical flow on the cavity floor. The vortical flow travels downstream and decelerates by the rear wall of the cavity which causes a severe increase in pressure. Both two- and three-dimensional results show the same trend as the experimental data. In fact, the lower pressures in three-dimensional cavity indicate that it is oscillating in shear layer mode and such a transition to wake mode is not observed in three-dimensional case which is consistent with the numerical investigation performed by Shieh and Morris [8]. The same as the previous case (two-dimensional open cavity with $L/D = 4$), the two-dimensional cavity showed a tendency to wake mode.

D. Three-Dimensional Cavity with Two Openings

Similar to the cylindrical cavities, the cavity with two openings develops an exclusive flow instability, which is fundamentally different from the Rossiter's concept. Pressure fluctuations and SPL spectra are shown at different locations in Fig. 17. Large pressure fluctuations, especially on the cavity floor, can be observed. The existence of the two openings changes the characteristics of flow over the cavity. Over a range of about 10^2–10^3 Hz (in logarithmic scale), the amplitude of the SPL remains on the order of 120–165 db, whereas at higher frequencies, it drops quickly. Based on the Rossiter formula for the cavity with$L/D = 2$, two empirical values were chosen as $k = 0.66$ and $\alpha = 0.25$. In the current operating conditions, frequencies for the first four modes, based on the Rossiter Formula, are $f_1 = 81.82$, $f_2 = 190.92$, $f_3 = 300.02$, and $f_4 = 409.12$ Hz. However, in this case, there are several fluctuations in SPL values, which are not similar to either open or closed cavities.

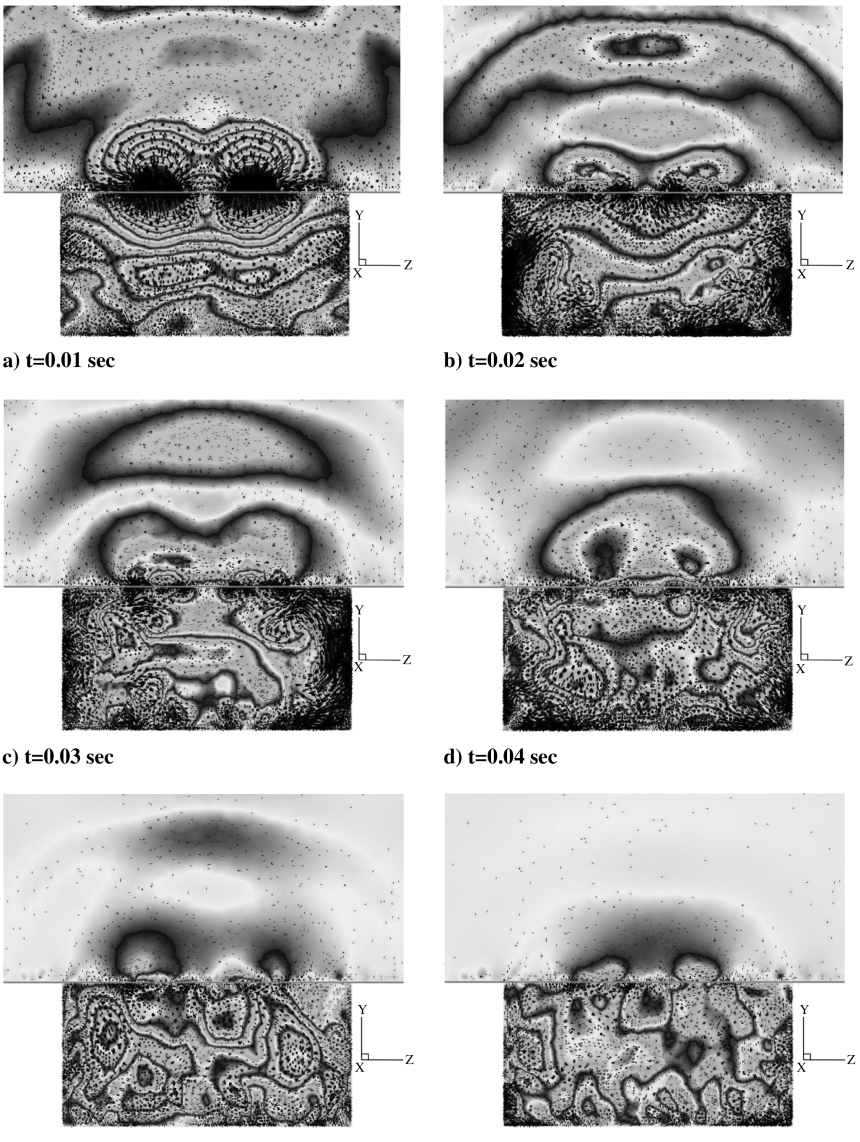

a) t=0.01 sec b) t=0.02 sec

c) t=0.03 sec d) t=0.04 sec

e) t=0.1 sec f) t=0.18 sec

Fig. 19 Snapshots of tangential vectors contoured with v-velocity (at $X = 0$ plane) of the three-dimensional cavity with two holes.

The SPL spectra show different characteristics of the flow depending on the geometry of the cavities. In the closed cavity, a large amount of fluctuation in pressure can be observed, while in the open cavity, some significant peaks can be seen. These peaks can be observed in a manner that is similar to open cavities, but they do not match the values calculated by the semi-empirical Rossiter formula.

Figure 18 shows the Schlieren-like pressure contours over the cavity at different time levels. The magnitudes of the pressure gradient yield these images, which are like Schlieren contours and provide insight into the flow characteristics and cavity noise. The acoustic radiations traveling upstream can be clearly observed. The acoustic field is three-dimensional and has a spherical radiation pattern.

Figure 19 illustrates the velocity field at different time steps. These snapshots show the rapid motion of the mixing layer over the cavity. The flow enters the cavity through the holes and generates vortical motion near the side walls and cavity floor. The flow inside the cavity is highly three-dimensional with vortical motion pattern. The vertical component of the velocity has a rapid back and forth motion which expedites the generation of the acoustic field. These vortical motions are coupled with the severe pressure fluctuations within the cavity. Part of this vortical flow exits the cavity from the holes and the other part remains within the cavity and brings up the vortices. It is clearly observed that after a while the intensity of the flow motion within the cavity is reduced and less acoustic radiations travel upstream.

The behavior of the flow over the cavity with two openings is related to the size of the holes, size of the cavity, and operating conditions.

V. Conclusions

Numerical simulations of subsonic and transonic turbulent flow over different types of cavities in two- and three- dimensional models were performed, and the results were compared with each other, available semi-empirical solutions, and experimental data. Turbulent flow simulation was performed with detached-eddy simulation using the SA one-equation model. In the two-dimensional closed cavity, only the broadband noise was observed in the SPL spectra. In this type of cavity, the random component of the pressure was more dominant than the periodic component. In the two-dimensional open cavity, the SPL spectra consisted of harmonic frequency peaks. In this case, the flow is dominated by periodic pressure fluctuations, while the random component is less significant. Transition to a wake mode was also observed in this type of the cavity. Another investigation was performed in a transonic regime to compare the flow behavior of the two- and three-dimensional open cavities. It was shown that the results of the three-dimensional cavity are in good agreement with the available experimental data, while there is a difference in the results of the two- and three-dimensional models. The amplitude of the pressure fluctuations in the two-dimensional case is larger than the three-dimensional model. Moreover, the pressure fluctuation of the two-dimensional cavity was more periodic than that of the three-dimensional case. However, it was observed that the trend of the pressure fluctuations of the two- and three-dimensional cavities was similar. The comparison of the two- and three-dimensional cavities indicates that the transition to wake mode does not occur in three- dimensional case and it is only oscillating in shear layer mode. Another cavity with two openings on top was investigated. Those results show that the existence of these holes changes the characteristics of the flow within the cavity. In fact, the resulting flow instability becomes a function of the size of the holes, size of the cavity, and operating conditions.

References

[1] Chung, K., "Characteristics of Compressible Rectangular Cavity Flows," *Journal of Aircraft*, Vol. 40, No. 1, Jan–Feb, 2003, pp. 137–142. doi:10.2514/2.3068.

[2] Rossiter, J. E., *Wind-Tunnel Experiments on the Flow over Rectangular Cavities at Subsonic and Transonic Speeds*, Aeronautical Research Council Reports and Memoranda, Rept. No. 3438, 1966.

[3] Sarohia, V., and Massier, P. F., "Control of Cavity Noise," *Journal of Aircraft*, Vol. 14, No. 9, Sept. 1977, pp. 833–837. doi:10.2514/3.58862.

[4] Krishnamurty, K., "Acoustic Radiation from Two-Dimensional Rectangular Cutouts in Aerodynamic Surfaces," NACA TN-3487, 1955.

[5] Heller, H. H., and Holmes, D. G., "Flow Induced Pressure Oscillations in Shallow Cavities," *Journal of Sound and Vibration*, Vol. 18, No. 4, 1971, pp. 545–553. doi:10.1016/0022-460X(71)90105-2.

[6] Gharib, M., and Roshko, A., "The Effect of Flow Oscillations on Cavity Drag," *Journal of Fluid Mechanics*, Vol. 177, No. 1, 1987, pp. 501–530. doi:10.1017/S002211208700106X.

[7] Rockwell, D., and Knisely, C., "The Organized Nature of Flow Impingement Upon a Corner," *Journal of Fluid Mechanics*, Vol. 93, No. 3, 1979, pp. 413–432. doi:10.1017/S0022112079002573.

[8] Shieh, C. M., and Morris, P. J., "Comparison of Two- and Three-Dimensional Turbulent Cavity Flows," in *39th AIAA Aerospace Sciences Meeting & Exhibit*, AIAA Paper 2001-0511, 2001.

[9] Lada, C., and Kontis, K., "Fluidic Control of Cavity Configurations at Subsonic and Supersonic Speeds," *43rd AIAA Aerospace Sciences Meeting and Exhibit*, AIAA Paper 2005-1298, 2005.

[10] Chang, K. S., and Park, S. O., "Hybrid RANS/LES Simulation of Deep Cavity Flow," *42nd AIAA Aerospace Sciences Meeting and Exhibit*, AIAA Paper 2004-53, 2004.

[11] Nayyar, P., Barakos, G. N., and Badcock, K. J., "Analysis and Control of Transonic Cavity Flow Using DES and LES," *35th AIAA Fluid Dynamics Conference and Exhibit*, AIAA Paper 2005-5267, 2005.

[12] Peng, S.-H., "Simulation of Turbulent Flow Past a Rectangular Open Cavity Using DES and Unsteady RANS," *24th Applied Aerodynamics Conference*, AIAA Paper 2006-2827, 2006.

[13] Kim, H. J., Aradag, S., and Knight, D. D., "Two and Three Dimensional Simulations of Supersonic Cavity Flow," *12th AIAA/CEAS Aeroacoustics Conference (27th AIAA Aeroacoustics Conference)*, AIAA Paper 2006-2431, 2006.

[14] Murray, N. E., and Ukeiley, L. S., "Flow Field Dynamics in Open Cavity Flows," in *12th AIAA/CEAS Aeroaucostics Conference (27th AIAA Aeroacoustics Conference)*, AIAA Paper 2006-2428, 2006.

[15] Boydston, J. D., and Squires, K. D., "Detached Eddy Simulation of High Reynolds Number Flow Over a Rectangular Cavity," *46th AIAA Aerospace Sciences Meeting and Exhibit*, AIAA Paper 2008-606, 2008.

[16] Langtry, R. B., and Spalart, P. R., "DES Investigation of a Baffle Device for Reducing Landing-Gear Cavity Noise," *46th AIAA Aerospace Sciences Meeting and Exhibit*, AIAA Paper 2008-13, 2008.

[17] Shieh, C. M., and Morris, P. J., "Parallel Numerical Simulation of Subsonic Cavity Noise," *5th AIAA/CEAS Aeroacoustics Conference*, AIAA Paper 99-1891, 1999.

[18] Rona, A., and Brooksbank, E. J., "POD Analysis of Cavity Flow Instability," in *41st AIAA Aerospace Sciences Meeting and Exhibit*, AIAA Paper 2003-178, 2003.

[19] Zhang, J., Morishitaf, E., Okunukil, T., and Itoh, H., "Experimental and Computational Investigation of Supersonic Cavity Flows," *AIAA/NAL-NASDA-ISAS 10th International Space Planes and Hypersonic Systems and Technologies Conference*, AIAA Paper 2001-1755, 2001.

[20] Zhang, K., and Naguib, A. M., "Dispersion Relation and Mode Selectivity in Low-Mach-Number Cavity Flows," *36th AIAA Fluid Dynamics Conference and Exhibit*, AIAA Paper 2006-3229, 2006.

[21] Little, J., Debiasi, M., and Samimy, M., "Flow Structure in Controlled and Baseline Subsonic Cavity Flows," *44th AIAA Aerospace Sciences Meeting and Exhibit*, AIAA Paper 2006-480, 2006.

[22] Vakili, A. D., and Gauthier, C., "Control of Cavity Flow by Upstream Mass-Injection," *Journal of Aircraft*, Vol. 31, No. 1, Jan–Feb, 1994, pp. 169–174. doi:10.2514/3.46470.

[23] Heo, D. N., and Lee, D. J., "Numerical Investigation of the Cover-Plates Effects on the Rectangular Open Cavity," in *7th AIAA/CEAS Aeroacoustics Conference*, AIAA Paper 2001-2127, Maastricht, The Netherlands, 28–30 May, 2001.

[24] Guo, Y. P., and Yamamoto, K. J., "Experimental Study on Aircraft Landing Gear Noise," *Journal of Aircraft*, Vol. 43, No. 2, March–April 2006, pp. 306–317. doi:10.2514/1.11085.

[25] Strang, W. Z., Tomaro, R. F., and Grismer, M. J., "Defining Methods of Cobalt60: A Parallel, Implicit, Unstructured Euler/Navier–Stokes Flow Solver," AIAA Paper 99-0786, 1999.

[26] Forsythe, J. R., Strang, W. Z., and Hoffmann, K. A., "Validation of Several Reynolds-Averaged Turbulence Models in a 3D Unstructured Grid Code," *Fluids 2000 Conference and Exhibit*,

AIAA Paper 2000-2552, 2000.
[27] Viswanathan, A. K., Squires, K. D., and Forsythe, J. R., "Detached Eddy Simulation of the Flow over an Axisymmetric Cavity," *41st Aerospace Sciences Meeting and Exhibit*, AIAA Paper 2003-265, 2003.
[28] Cobalt User's Manual, Ver. 3.0, Cobalt Solution, LLC, Springerfield, OH, 2003.
[29] Spalart, P. R., Jou, W. H., Strelets, M., and Allmaras, S. R., "Comments on the Feasibility of LES for Wings, and on a Hybrid RANS/LES Approach," in *Advance in DNS/LES, 1st AFOSR International Conference on DNS/LES*, Greyden Press, Columbus, OH, 1997.
[30] Squires, K. D., "Detached-Eddy Simulation: Current Status and Perspectives," *Proceedings of Direct and Large-Eddy Simulation-5*, Kluwer Academic, Norwell, MA, 2004.
[31] Piomelli, U., Radhakrishnan, S., and Prisco, G. D., "Turbulent Eddies in the RANS/LES Transition Region," *Advances in Hybrid RANS-LES Modelling*, Vol. 97, 2008, pp. 21–36.
doi:10.1007/978-3-540-77815-8_3
[32] Doran, D., "Experimental Investigation of Transonic Cavity Flow Control," MS Thesis, School of Engineering, Cranfield Univ., 2006.
[33] Dietiker, J. F., and Hoffmann, K. A., "Computations of Turbulent Flow over a Backstep," *37th AIAA Fluid Dynamics Conference and Exhibit*, AIAA Paper 2007-3862, 2007.
[34] Wagner, C., Huttl, T., and Sagaut, P., *Large-Eddy Simulation for Acoustics*, Cambridge Univ. Press, New York, 2007.
[35] Heller, H. H., and Bliss, D. B., "Physical Mechanism of Flow Induced Pressure Fluctuations in Cavities and Concepts of their Suppression," *AIAA 2nd Aeroacoustics Conference*, AIAA Paper 75-491, 1975.
[36] Tracy, M. B., and Plentovich, E. B., "Characterization of Cavity Flow Fields Using Pressure Data Obtained in the Langley 0.3-Meter Transonic Cryogenic Tunnel," NASA Technical Paper 4436, 1993.
[37] Rowley, C. W., "Modeling, Simulation, and Control of Cavity Flow Oscillations," Doctoral Thesis, Department of Mechanical Engineering, California Inst. of Technology, Pasadena, CA, 2002.
[38] Rowley, C. W., Colonius, T., and Basu, A. J., "On Self-Sustained Oscillations in Two-Dimensional Compressible Flow over Rectangular Cavities," *Journal of Fluid Mechanics*, Vol. 455, pp. 315–346.
[39] Roshko, A., "*Some Measurements of Flow in a Rectangular Cutout*," NACA TN 3488, 1955.
[40] Colonius, T., Basu, A. J., and Rowley, C. W., "Numerical Investigation of the Flow Past a Cavity," *5th AIAA/CEAS Aeroacoustics Conference*, AIAA Paper 1999-1912, 1999.
[41] Chung, K. M., "Characteristics of Transonic Rectangular Cavity Flows," *Journal of Aircraft*, Vol. 37, No. 3, May–June 2000, pp. 463–468.
doi:10.2514/2.2620.
[42] Baysal, O., and Stallings, R. L. J., "Computational and Experimental Investigation of Cavity Flowfields," *AIAA Journal*, Vol. 26, No. 1, 1988, pp. 6–7.
doi:10.2514/3.9842.
[43] Henshaw, M. J., "M219 Cavity Case, in Verification and Validation Data for Computational Unsteady Aerodynamics," RTO Tech Rept. TR-26, AC/323 (AVT) TP/19, pp. 453–472.